2
4-20-77

LA-6673-MS
Informal Report

Special Distribution

Issued: March 1977

H(t,t)H Scattering at Low Energies

by

R. F. Haglund, Jr.
D. Fick*
P. A. Schmelzbach**
G. G. Ohlsen
Nelson Jarmie
Ronald E. Brown***

*Visiting Staff Member, Max-Planck Institut fur Kernphysik, Heidelberg, West Germany.
**Visiting Staff Member, Eidgenossische Technische Hochschule, Zurich, Switzerland.
***Visiting Staff Member, University of Minnesota, Minneapolis, MN 55455.

los alamos
scientific laboratory
of the University of California
LOS ALAMOS, NEW MEXICO 87545

An Affirmative Action/Equal Opportunity Employer

UNITED STATES
ENERGY RESEARCH AND DEVELOPMENT ADMINISTRATION
CONTRACT W-7405-ENG. 36

DISTRIBUTION OF THIS DOCUMENT IS UNLIMITED

MASTER

H($\vec{t}$,t)H SCATTERING AT LOW ENERGIES

by

R. F. Haglund, Jr., D. Fick, P. A. Schmelzbach, G. G. Ohlsen,
Nelson Jarmie, and Ronald E. Brown

ABSTRACT

We present angular distributions of the differential cross section and vector analyzing power for H + $\vec{t}$ elastic scattering, at center-of-mass energies 1.26, 1.68, 2.19, 2.70, 3.21, and 3.71 MeV. A preliminary phase-shift analysis of the data confirms the importance of the odd-parity tensor and even-parity spin-orbit nucleon-nucleon forces in model calculations for the ^{4}He system in this energy range.

I. INTRODUCTION

The high symmetry of the ^{4}He nucleus makes it an object of considerable theoretical and experimental interest. In particular, the symmetries of the nuclear wave functions for the excited states of ^{4}He allow us to draw inferences about individual components of the nucleon-nucleon interaction. In this report, we present experimental data and a preliminary analysis bearing on the even-parity spin-orbit and odd-parity tensor components of the internucleon force.

Foldy and Walecka have shown[1] that the negative-parity excited states of ^{4}He (see Fig. 1) can be viewed as the [15]-dimensional representation of SU(4) in Wigner's supermultiplet theory.[2] This degenerate supermultiplet is split by the spin-dependent parts of the nucleon-nucleon interaction—namely, the spin-orbit force, the tensor force, and the difference between singlet and triplet central forces.[3] In the present work, we shall be concerned primarily with the 0^-, T = 0 level (21.1 MeV) and the 2^-, T = 0 level (22.1 MeV),[4] which are split by a delicate balance between the tensor and spin-orbit forces.[5]

NOTICE
This report was prepared as an account of work sponsored by the United States Government. Neither the United States nor the United States Energy Research and Development Administration, nor any of their employees, nor any of their contractors, subcontractors, or their employees, makes any warranty, express or implied, or assumes any legal liability or responsibility for the accuracy, completeness or usefulness of any information, apparatus, product or process disclosed, or represents that its use would not infringe privately owned rights.

Because spin-dependent forces are required to split the odd-parity levels, model calculations cannot be thoroughly tested without data on spin-dependent observables. In the case of the 0^- and 2^- levels, this requires polarization and/or analyzing powers from ^{3}He + n or ^{3}H + p elastic scattering or the ^{3}H(p,n)^{3}He reaction, since the ^{3}H + d threshold lies above both levels (Fig. 1). Previous measurements in or near the energy range of interest include ^{3}H + $\vec{p}$ elastic scattering down to about 3.11 MeV c.m. energy[6] (22.93 MeV excitation energy in ^{4}He) and a very limited set of angular distributions for H + t polarization in the range from 1.60 to 2.41 MeV c.m. energy[7] (21.42 to 22.23 MeV excitation energy).

The paucity of data at energies corresponding to the neighborhood of the 0^- and 2^- levels motivated the experiment described here. Six angular distributions of the differential cross section and analyzing power for ^{1}H + t elastic scattering were measured between 1.26 and 3.71 MeV c.m. energy (21.08 to 23.53 Mev excitation energy in ^{4}He). Analysis of these data appears to confirm Hackenbroich's conjecture[8] that the ordering of the 0^- and 2^- levels can be predicted correctly by the refined cluster

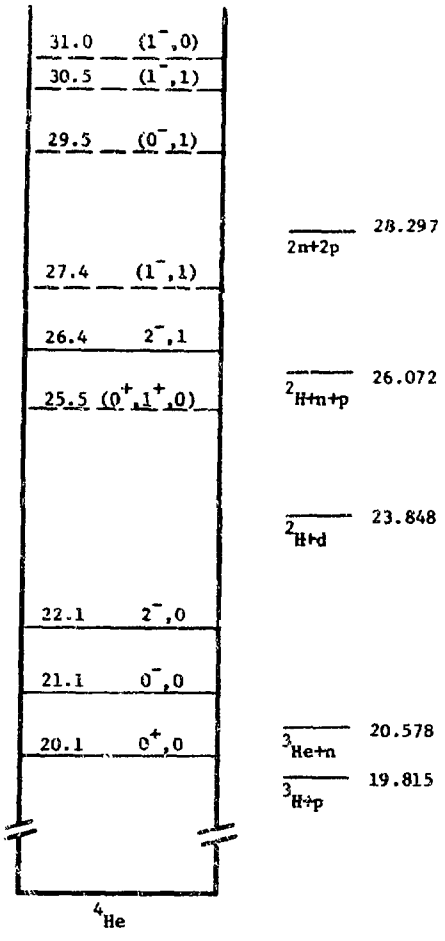

Fig. 1.
Level scheme for the ^{4}He system.

model[9]—provided that the "small" (and previously neglected) components of the nucleon-nucleon spin-orbit and tensor forces are included in the cluster-model Hamiltonian.

II. EXPERIMENTAL DETAILS

The polarized-triton source[10] and the Los Alamos Model FN tandem Van de Graaff accelerator were used in this experiment. Triton beam currents averaged 30 nA on target, with an average polarization of 0.78. Beam polarization was monitored by the quench ratio technique.[10]

Angular distributions of the cross section and analyzing powers were measured at triton energies of 5.03, 6.71, 8.76, 10.80, 12.82, and 14.84 MeV, corresponding respectively to c.m. energies of 1.26, 1.68, 2.19, 2.70, 3.21, and 3.71 MeV.

A 300° circular gas target containing hydrogen gas was mounted in the "Supercube" scattering chamber,[11] as shown in Fig. 2. The entrance foil for the target was 2.5-μm Havar;* an exit foil of 2.5-μm Havar was used for all angular distributions except that at 5.03 MeV triton energy. At this lowest energy, a 6.3-μm Kapton* foil was used to reduce multiple scattering of the particles leaving the gas cell. The target was filled to a nominal pressure of 300 torr, as measured on a Wallace-Tiernan gauge outside the scattering chamber.

A single pair of detectors or detector telescopes was mounted at equal angles, right and left of the incident beam, as shown in Fig. 2. For detecting recoil protons with incident beam energies between 9 and 15 MeV, 1000-μm-thick, 150-mm² detectors were used as singles counters, with the bias reduced as appropriate to lower the effective thickness of the counter. At forward angles in this energy range, particle telescopes were used to permit on-line mass identification.[12] For this mode of operation, we used 86.5-μm-thick, 150-mm² ΔE counters followed by 1000-μm-thick E counters. At a triton bombarding energy of 7 MeV, the recoil protons were detected using the 86.5-μm detectors in singles mode. For the forward-angle data at 7 MeV and for all the data obtained at 5.03 MeV, we used counter telescopes containing 17-μm-thick, 50-mm² ΔE and 300-μm-thick E silicon surface-barrier detectors.

At all energies, we used a slit system consisting of a front slit, two antiscattering slits, and a rear slit (see Fig. 2). Both front and rear slits were nominally 3.33 mm wide (1° FWHM). For the energies where we used 150-mm² detectors, the rear slit was 11.4 mm high. At 6.71 and 5.03 MeV, where 50-mm² ΔE detectors were used, the rear-slit height was reduced to 6.25 mm to insure that all particles entering the rear slit would strike the active area of the ΔE crystal.

At each energy and angle, the yield in the left and right detection systems was measured, for a preset

*Havar is the trade name for a cobalt "superalloy" manufactured by Hamilton Technology, Inc., Lancaster, Pa. Kapton is a polyimide film made by E. I. duPont de Nemours and Company, Wilmington, DE.

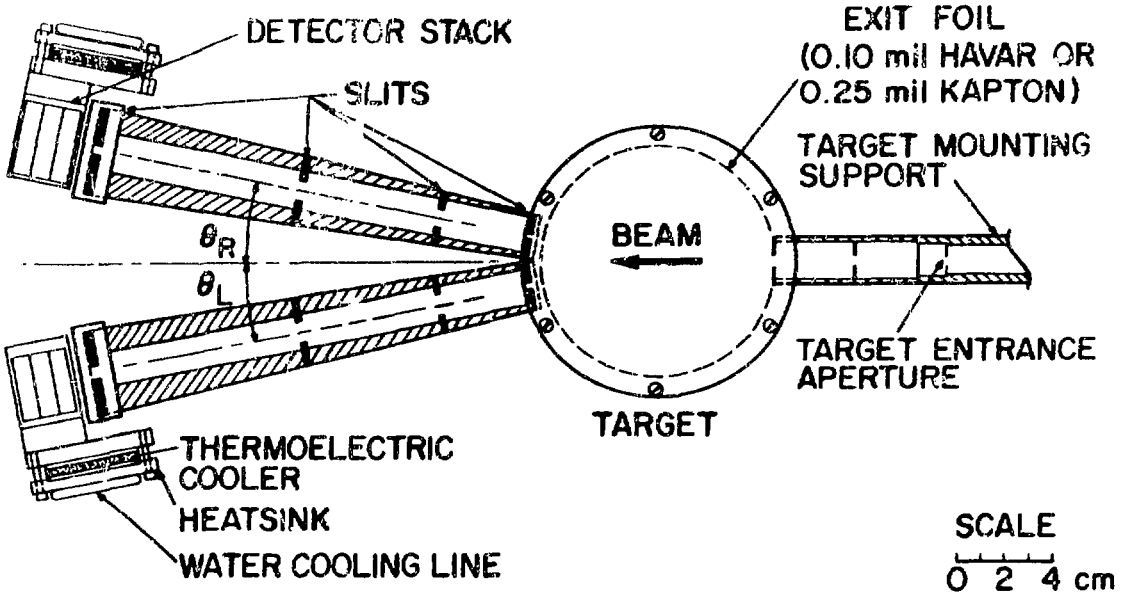

Fig. 2.
Schematic of the experimental layout, showing the gas target, collimation system, and location of detectors.

integrated charge, with the spin orientation of the beam up and down. The geometric means L and R of the integrated peak sums for each detector were constructed according to the prescription

$$L = [\text{Left (spin up)} \cdot \text{Right (spin down)}]^{1/2}$$

$$R = [\text{Right (spin up)} \cdot \text{Left (spin down)}]^{1/2} \quad (1)$$

The analyzing power A_y and the lab differential cross section σ_o are then given by[18]

$$A_y = \frac{1}{P} \cdot \frac{L-R}{L+R} \quad (2)$$

$$\sigma_o = \frac{(L+R)\sin\theta_o}{2nNG}, \quad (3)$$

where P is the average beam polarization, θ_o is the lab angle, n is the number of beam particles, N is the number of target particles, and G is the usual gas-target geometry factor.[14]

III. EXPERIMENTAL RESULTS

The energy spectra for all the experimental data points were analyzed off-line using the SDS-930 computer. Background gates—either linear or exponential, as appropriate—were set, by taking a visual best fit to the observed background. The background-subtracted peaks were then used to compute the geometric mean yields, analyzing powers, and differential cross sections.

Angular distributions of the differential cross sections are given in Table I to VI and in Fig. 3. Only relative errors are shown. There are numerous contributions to the relative error; a good summary may be found in Ref. 15. In the present case, the most significant sources of error are (1) errors in background subtraction and (2) errors in our knowledge of the target gas pressure.

The magnitude of errors due to (1) is variable, but never worse than 3%. The error due to (2), which results from uncertainties in reading the Wallace-Tiernan gauge, is estimated to be 1%. This corresponds to an uncertainty of ±3 torr in the gauge

TABLE I

CENTER-OF-MASS DIFFERENTIAL CROSS SECTION σ AND ANALYZING POWER A_y for $H(\vec{t},t)H$ ELASTIC SCATTERING AT E_{CM} = 1.26 MeV

Lab Angle (deg)	c.m. Angle (deg)	σ (mb/sr)	Δσ (%)	A_y	ΔA_y
12.00[a]	50.50	---	---	0.259	0.005
13.00[a]	55.35	---	2.0	0.272	0.005
14.00[a]	60.45	161.1	2.0	0.277	0.005
15.00[a]	65.80	150.0	2.0	0.276	0.005
16.00[a]	71.65	139.7	---	0.254	0.005
50.00[b]	79.95	---	2.0	0.184	0.010
47.50	84.95	121.5	2.0	0.127	0.009
45.00	89.95	126.1	2.0	0.086	0.009
42.50	94.95	127.2	2.0	0.039	0.009
40.00	99.95	133.6	2.0	−0.017	0.008
37.50	104.95	137.8	2.0	−0.066	0.008
35.00	109.95	152.0	2.0	−0.098	0.008
32.50	114.95	165.5	2.0	−0.120	0.008
30.00	119.95	179.1	2.0	−0.135	0.007
27.50	124.95	192.7	2.0	−0.136	0.007
25.00	129.95	208.7	2.0	−0.137	0.007
22.50	134.95	224.5	2.0	−0.147	0.007
20.00	139.95	240.1	2.0	−0.125	0.005
17.50	144.95	261.6	2.0	−0.122	0.009
16.00	147.95	260.0	2.0	−0.117	0.008
15.00	149.95	269.5	2.0	−0.110	0.007
14.00	151.95	277.2	2.0	−0.104	0.007
13.00	153.95	---	---	−0.086	0.007
12.00	155.95	---	---	−0.078	0.007

[a]Triton detected with particle identification.

[b]Weighted average of triton and recoil proton point at the same c.m. angle. For all other data, the recoil proton was detected with particle identification.

reading. In addition, we found some discrepancies between singles and telescope yields at the same energies. This indicates an additional, though unknown, source of relative error, which we estimate to be ±2.5%.

The scale error arises from uncertainty in the overall normalization of the data. The data from 8.76 to 14.84 MeV were normalized to the work of Ivanovich et al.,[16] while the lowest energy angular distributions were normalized to the data of Ennis and Hemmendinger.[17] In both cases, we assign a scale error of 3% due to the normalization.

No cross sections are given for laboratory angles forward of 13.0°, because the detector snouts begin to cut into the triton beam leaving the gas cell. This does not affect the measured analyzing powers.[18] However, it does reduce the current reaching the

TABLE II

CENTER-OF-MASS DIFFERENTIAL CROSS SECTIONS σ AND ANALYZING POWER A_y FOR $H(\vec{t},t)H$ ELASTIC SCATTERING AT E_{CM} = 1.68 MeV

Lab Angle (deg)	c.m. Angle (deg)	σ (mb/sr)	Δσ (%)	A_y	ΔA_y
11.00[a]	45.85	---	---	0.31	0.01
12.00[a]	50.50	---	---	0.34	0.01
13.00[a]	55.35	---	---	0.37	0.01
14.00[a]	60.45	192.7	3.0	0.40	0.01
15.00[a]	65.80	160.3	3.0	0.44	0.01
16.00[a]	71.65	139.6	3.0	0.49	0.01
16.50[a]	74.85	132.4	3.0	0.50	0.01
52.50	74.90	---	3.0	0.495	0.010
50.00	79.90	102.6	3.0	0.508	0.010
47.50	84.90	103.2	3.0	0.485	0.010
45.00	89.90	99.3	3.0	0.479	0.018
42.50	94.90	101.9	3.0	0.432	0.010
40.00	99.90	101.8	3.0	0.387	0.010
37.50	104.90	105.2	3.0	0.33	0.01
35.00	109.90	116.2	3.0	0.266	0.010
32.50	114.90	124.7	3.0	0.20	0.01
32.00	115.90	126.3	3.0	0.18	0.01
30.00	119.90	150.0	3.0	0.16	0.01
27.50	124.90	163.0	3.0	0.11	0.01
25.00	129.95	---	3.0	0.08	0.01
22.50	134.95	---	3.0	0.05	0.01
18.00[b]	143.95	230.6	3.0	0.025	0.008
17.50[b]	144.9[illegible]	234.0	3.0	0.026	0.008
17.00[b]	145.95	232.0	3.0	0.026	0.008
16.50[b]	146.95	240.5	3.0	0.028	0.007
16.00[b]	147.95	244.6	3.0	0.029	0.008
15.00[b]	149.95	251.8	3.0	0.028	0.007
14.00[b]	151.95	275.3	3.0	0.027	0.007
13.00[b]	153.95	---	3.0	0.013	0.007
12.00[b]	155.95	---	3.0	0.014	0.007
11.00[b]	157.95	---	3.0	0.012	0.005

[a]Tritons detected with particle identification.

[b]Recoil protons detected with particle identification. For all other data, the recoil protons were detected in singles mode.

TABLE III

CENTER-OF-MASS DIFFERENTIAL CROSS SECTION σ AND ANALYZING POWER A_y FOR $H(\vec{t},t)H$ ELASTIC SCATTERING AT E_{CM} = 2.19 MeV

Lab Angle (deg)	c.m. Angle (deg)	σ (mb/sr)	Δσ (%)	A_y	ΔA_y
11.00[a]	45.85	---	---	0.132	0.005
12.50[a]	52.95	---	---	0.154	0.005
13.75[a]	59.20	195.7	5.6	0.180	0.005
60.00	59.90	---	---	0.19	0.01
57.50	64.90	---	---	0.22	0.01
15.00[a]	65.80	159.2	5.6	0.224	0.005
55.00	69.90	---	---	0.25	0.01
52.50	74.90	121.6	2.9	0.27	0.01
50.00	79.90	109.3	2.8	0.32	0.01
47.50	84.90	96.9	2.7	0.36	0.01
45.00	89.90	85.8	2.9	0.41	0.01
42.50	94.90	79.8	2.8	0.44	0.01
40.00	99.90	76.2	2.7	0.47	0.01
37.50	114.90	76.4	2.7	0.46	0.01
35.00	109.90	79.4	2.7	0.45	0.01
32.50	114.90	85.1	2.7	0.40	0.01
30.00	119.90	92.4	2.7	0.36	0.01
27.50	124.90	103.4	2.7	0.31	0.01
25.00	129.90	112.2	2.7	0.26	0.01
22.50	134.90	126.0	2.7	0.21	0.01
20.00[b]	139.95	153.4	5.6	0.190	0.006
17.50[b]	144.95	166.7	5.6	0.159	0.007
15.00[b]	149.95	177.1	5.6	0.133	0.008
13.75[b]	152.45	193.9	5.6	0.109	0.007
12.50[b]	154.95	---	---	0.097	0.007
11.00[b]	157.95	---	---	0.082	0.006

[a]Triton detected with particle identification.

[b]Recoil proton detected with particle identification. For all other data, the recoil proton was detected in singles mode.

TABLE IV

CENTER-OF-MASS DIFFERENTIAL CROSS SECTION σ AND ANALYZING POWER A_y FOR $H(\vec{t},t)H$ ELASTIC SCATTERING AT E_{CM} = 2.70 MeV

Lab Angle (deg)	c.m. Angle (deg)	σ (mb/sr)	Δσ (%)	A_y	ΔA_y
11.00[a]	45.85	---	---	0.033	0.005
12.50[a]	52.95	---	---	0.040	0.005
13.75[a]	59.20	194.5	5.6	0.045	0.005
60.00	59.90	193.4	3.1	0.06	0.01
57.50	64.90	147.7	3.1	0.07	0.01
15.00[a]	65.30	158.5	5.6	0.071	0.005
55.00	69.90	137.6	3.0	0.08	0.01
52.50	74.90	119.2	2.8	0.11	0.01
50.00	79.90	103.6	2.8	0.14	0.01
17.50[a]	81.90	---	---	0.154	0.005
47.50	84.90	85.9	2.9	0.20	0.01
45.00	89.90	73.1	2.7	0.26	0.01
42.50	94.90	63.7	2.7	0.32	0.01
40.00	99.90	58.5	2.7	0.39	0.01
37.50	104.90	57.2	2.7	0.43	0.01
35.00	109.90	58.2	2.7	0.45	0.01
32.50	114.90	63.0	2.7	0.43	0.01
30.00	119.90	68.7	2.7	0.40	0.01
27.50	124.90	77.7	2.7	0.36	0.01
25.00	129.90	88.9	2.7	0.32	0.01
22.50	134.90	100.2	3.0	0.28	0.01
20.00[b]	139.95	119.9	5.7	0.247	0.007
17.50[b]	144.95	130.4	5.6	0.213	0.007
15.00[b]	149.95	144.4	5.6	0.169	0.007
13.75[b]	152.45	153.4	5.6	0.150	0.008
12.50[b]	154.95	---	---	0.136	0.007
11.00[b]	157.95	---	---	0.112	0.006

[a]Triton detected with particle identification.

[b]Recoil proton detected with particle identification. For all other data, the recoil proton was detected in singles mode.

TABLE V

CENTER-OF-MASS DIFFERENTIAL CROSS SECTION σ AND ANALYZING POWER A_y FOR $H(\vec{t},t)H$ ELASTIC SCATTERING AT $E_{c.m.}$ = 3.21 MeV

Lab Angle (deg)	c.m. Angle (deg)	σ (mb/sr)	Δσ (%)	A_y	ΔA_y
11.00[a]	45.85	---	---	−0.020	0.005
12.50[a]	52.95	---	---	−0.019	0.005
13.75[a]	59.20	191.1	5.6	−0.022	0.005
60.00	59.85	---	---	−0.02	0.01
57.50	64.85	---	---	−0.01	0.01
15.00[a]	65.80	153.2	5.6	−0.014	0.005
55.00	69.85	130.1	3.2	0.00	0.01
52.50	74.85	112.2	2.8	0.01	0.01
16.75[a]	76.50	104.5	5.6	0.014	0.005
50.00	79.85	94.0	2.8	0.03	0.01
17.50[a]	81.90	85.0	5.6	0.042	0.005
47.50	84.85	78.7	2.7	0.08	0.01
45.00	89.85	65.5	2.7	0.13	0.01
42.50	94.85	55.1	2.7	0.21	0.01
40.00	99.85	47.9	2.7	0.29	0.01
37.50	104.85	44.7	2.7	0.37	0.01
35.00	109.85	45.0	2.7	0.42	0.01
32.50	114.90	48.2	2.7	0.44	0.01
30.00	119.90	53.6	2.7	0.41	0.01
27.50	124.90	63.0	2.7	0.37	0.01
25.00	129.90	71.5	2.7	0.33	0.01
22.50	134.90	83.4	2.8	0.30	0.01
20.00	139.90	---	---	0.27	0.01
17.50[b]	144.90	115.0	5.6	0.213	0.008
16.25[b]	146.40	117.0	5.6	0.193	0.007
15.00[b]	149.90	124.4	5.6	0.173	0.009
13.75[b]	152.45	134.8	5.6	0.165	0.009
12.50[b]	154.95	---	---	0.138	0.008
11.00[b]	157.95	---	--	0.122	0.007

[a]Triton detected with particle identification.

[b]Recoil proton detected with particle identification. For all other data, the recoil proton was detected in singles mode.

TABLE VI

CENTER-OF-MASS DIFFERENTIAL CROSS SECTION σ AND ANALYZING POWER A_y FOR $H(\vec{t},t)H$ ELASTIC SCATTERING AT E_{CM} = 3.71 MeV

Lab Angle (deg)	c.m. Angle (deg)	σ (mb/sr)	$\Delta\sigma$ (%)	A_y	ΔA_y
11.00[a]	45.85	---	---	−0.047	0.005
12.50[a]	52.95	---	---	−0.060	0.005
62.00	55.85	---	---	−0.07	0.01
13.75[a]	59.20	186.7	5.6	−0.073	0.005
60.00	59.85	---	---	−0.07	0.01
58.00	63.85	173.2	2.9	−0.07	0.01
15.00[a]	65.80	150.4	5.6	−0.075	0.005
56.00	67.85	144.1	3.6	−0.07	0.01
54.00	71.85	124.1	2.9	−0.07	0.01
52.00	75.85	109.1	2.8	−0.07	0.01
50.00	79.85	94.0	2.7	−0.04	0.01
17.50[a]	81.70	81.4	5.6	−0.037	0.005
48.00	83.85	78.4	2.7	−0.02	0.01
46.00	87.85	65.5	2.7	0.01	0.01
44.00	91.85	54.3	2.7	0.07	0.01
42.00	95.85	46.2	2.7	0.14	0.01
40.00	99.85	40.3	2.7	0.22	0.01
38.00	103.85	36.5	3.0	0.30	0.01
36.00	107.85	35.7	2.9	0.38	0.01
34.00	111.85	36.7	2.8	0.44	0.01
32.00	115.85	39.6	2.7	0.46	0.01
30.00	119.85	44.1	2.7	0.44	0.01
28.00	123.85	50.2	2.7	0.42	0.01
26.00	127.85	58.2	2.7	0.39	0.01
24.00	131.85	67.3	2.7	0.34	0.01
22.00	135.90	75.3	2.8	0.31	0.01
21.00	137.90	86.2	2.9	0.29	0.01
20.00[b]	139.90	85.6	4.0	0.278	0.008
17.50[b]	144.90	101.4	5.6	0.223	0.008
15.00[b]	149.90	108.8	5.6	0.179	0.10
13.75[b]	152.45	114.9	5.6	0.158	0.009
12.50[b]	154.95	---	---	0.134	0.008
11.00[b]	157.95	---	---	0.122	0.007

[a]Triton detected with particle identification.

[b]Recoil proton detected with particle identification. For all other data, the recoil proton was detected in singles mode.

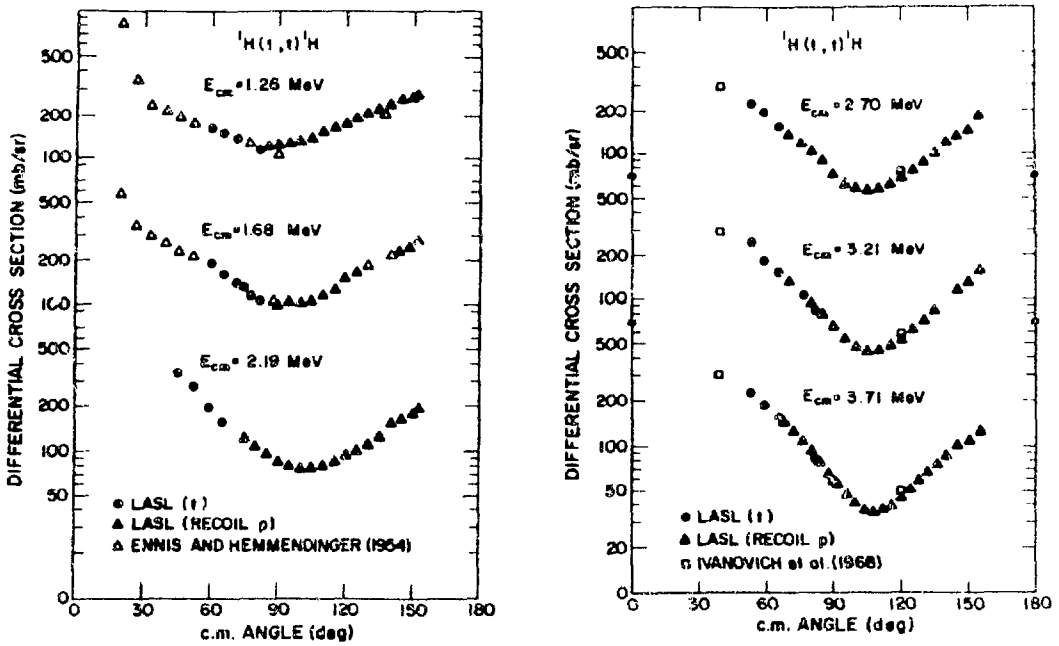

Fig. 3.
Absolute c.m. differential cross sections for $H(\vec{t},t)H$ at the indicated c.m. energies. Statistical errors are smaller than the plotting symbols.

Faraday cup, resulting in too high an apparent cross section.

Analyzing power angular distributions are listed in Tables I to VI, and shown in Fig. 4. Only relative errors are shown there. These are calculated by adding in quadrature: (1) the statistical error in the background-subtracted peak sum, (2) the random error in the selection of the background gates, (3) the random error in the measurement of the beam polarization using the quench ratio method, and (4) the random systematic error arising, for example, from position instability in the incident beam. In the present experiment, the largest source of error is believed to be (2). Based on our experience with reproducibility of the data for experiments of this type, we believe the error due to (4) to be 0.005.

The scale error for the analyzing power is estimated to be about 0.02 ± 2.0%. There are two principal sources of this scale error. The first is the presence of unpolarized, negatively charged background in the beam arising under certain conditions in the polarized-triton source.[16] The usual electric-field quench-ratio measurement of beam polarization includes this background beam with the "good" polarized beam. Hence, polarization values determined from electric-field quench-ratio measurements tend to be slightly too large—with a range of 0.01 to 0.02 above the (true) magnetic-field quench-ratio value. The second source of scale error is the slight negative polarization of the background (quenched) beam.[19] This second effect tends to compensate for the first, thus lowering slightly the scale error from the 0.02 maximum error associated with the negatively charged unpolarized background. A third source of error is polarization enhancement due to slit-edge scraping of the beam between the analyzing magnet beam stop (where the quench-ratio measurement is taken) and the target.[18] This effect contributes at most 0.01 to the polarization and tends to compensate for the error due to the electric-field quenching technique.

The energy uncertainty for the angular distributions ranges from ±20 keV at 5.03 MeV to ±10 keV at 14.84 MeV. The dominant contribution is the uncertainty in the thickness of the Havar entrance foil of the gas cell, which is estimated to be ±10%. The

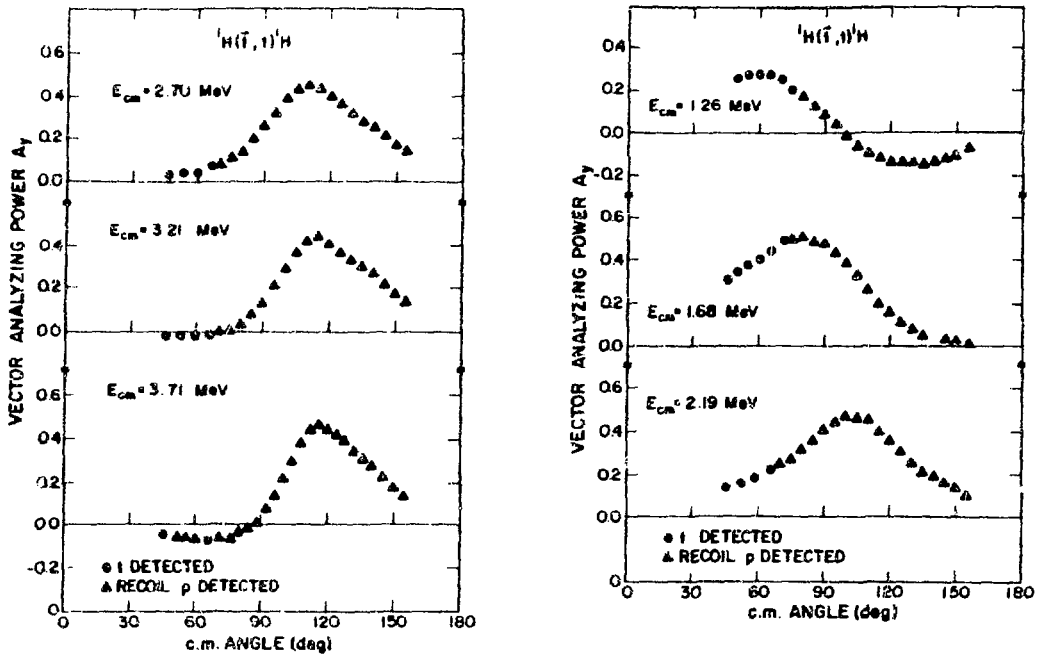

Fig. 4.
Vector analyzing powers for $H(\vec{t},t)H$ at the indicated c.m. energies. Statistical errors are smaller than the plotting symbols.

calibration of the analyzing magnet is based on a measurement of $^{13}C(p,p)^{13}C$ elastic scattering near the isospin-forbidden resonance at 14.2308 ± 0.0002 MeV (Refs. 19 and 20) and is believed to be accurate to within ±1 keV. The uncertainty in the linearity of the analyzing magnet is estimated to be ±3 keV. The error in the energy-loss calculations is believed to be at most 1% in this energy range. The overall energy uncertainty is the quadratic sum of the contributions from these four sources.

The energy spread of the incident beam arises primarily from straggling in the Havar entrance foil of the gas cell and in the target gas. Bohr's energy-independent straggling formula[21] gives energy spreads of 30 keV FWHM and 17.5 keV FWHM in the Havar and the target gas, respectively. When these two quantities are folded quadratically with the ±4 keV FWHM terminal ripple of the Van de Graaff, we obtain a nominal energy spread of 35 keV FWHM.

Other errors—e.g., relative detector efficiencies and relative integrated charge—are known to cancel exactly for analyzing power measurements made with symmetric geometry and proper spin flips.[13]

IV. NUCLEON-NUCLEON FORCES IN THE CLUSTER MODEL

The refined cluster model[9] uses realistic nucleon-nucleon potentials in a many-body Hamiltonian to predict observables and S-matrix elements for few-nucleon scattering and reaction problems. For elastic scattering, the S-matrix elements are related to the Blatt-Biedenharn phase shifts[22] δ^J_{LS} by

$$S^J_{LS} = \exp[2i\delta^J_{LS}] \quad , \tag{5}$$

where J is the total angular momentum, L is the orbital angular momentum, and S is the spin. The cluster-model phase shifts, in turn, may be compared to the phase shifts obtained from phenomenological fits to experimental data. From such a comparison, then, one may make inferences

about the role played by different components of the nucleon-nucleon force.

If one assumes that spin S, isospin T, and orbital angular momentum ℓ may be used to characterize the contributions to the potential, the nucleon-nucleon forces used for the cluster-model calculation may be divided up as shown in Table VII. The "large" forces at the energies of the present experiment are the even central, even tensor, and odd spin-orbit forces (labelled v_c^+, v_T^+, and v_{LS}^-, respectively), while the odd central, odd tensor, and even spin-orbit forces (v_c^-, v_T^-, and v_{LS}^+) are "small."[23] The relative smallness of the odd-parity central force arises from the exclusion principle. The even spin-orbit force vanishes for $\ell = 0$, and is much smaller for $\ell = 2$ than the odd spin-orbit force for $\ell = 1$. The lowest order even tensor force will mix $\ell = 0$ and $\ell = 2$, and is large compared to the lowest order odd tensor force, which mixes $\ell = 1$ and $\ell = 3$.

Extensive microscopic calculations for p + T and n + ^{3}He elastic scattering and for the T(p,n)^{3}He reaction have been published by Heiss and Hackenbroich[24] (hereafter referred to as H73). These calculations agree generally with the elastic scattering data above 3 MeV c.m. energy. However, the p-wave cluster-model phases of H73 do not agree with the phenomenological p-wave phases calculated from the data. The present data, as we shall now see, provide an experimental basis for the resolution of this discrepancy.

V. PHASE-SHIFT ANALYSIS

The most comprehensive phase-shift analysis of p-T scattering to date is that of Kankowsky et al.[6] This work is based upon ^{3}H($\vec{p}$,p)^{3}H elastic scattering in the energy range E_p = 4.5 - 12.0 MeV, corresponding to center-of-mass energies from 3.4 to 9.0 MeV. For the s-wave and singlet p-wave phases, the phenomenological analysis of Kankowsky et al. and the cluster-model calculations of H73 agree quite well. However, there is a substantial disagreement in the triplet p-wave phases—with H73 predicting phase shifts which lead to the wrong level-ordering in ^{4}He. Heiss and Hackenbroich give $\delta_{11}^2 > \delta_{11}^1 > \delta_{11}^0$ (in the notation δ_{LS}^J), which implies a level-ordering of 2^-, 1^-, 0^-, while the actual level sequence is 0^-, 2^-, 1^-. As observed by Kankowsky et al.,[6] this was probably due to neglect or improper choice of the odd-parity tensor force, which is known to play an important role in the splitting of the negative-parity levels in ^{4}He despite its relatively small magnitude.[5]

In response to this argument, Hackenbroich showed[8] that inclusion of reasonable even spin-orbit and odd tensor nucleon-nucleon forces in his cluster-model calculations could force a resonance in the 0^- triplet p-wave phase (δ_{11}^0) at low c.m. energies. These new calculations (referred to hereafter as H76) give $\delta_{11}^0 > \delta_{11}^2 > \delta_{11}^1$, and thus correspond to the proper level-ordering. However, there were at the time no p-T elastic scattering data at low enough

TABLE VII

RELATIVE STRENGTHS OF COMPONENTS OF NUCLEON-NUCLEON POTENTIAL

Spin S	Isospin T	ℓ	"Large" Forces	"Small" Forces
↑↑	↑↑	1,3,...	$V_{LS}^-(r)$	$V_c^-(r), V_T^-(r)$
↑↑	↑↓	0,2,...	$V_c^+(r), V_T^+(r)$	$V_{LS}^+(r)$
↑↓	↑↓	1,3,...	$V_{LS}^-(r)$	$V_c^-(r), V_T^-(r)$
↑↓	↑↑	0,2,...	$V_c^+(r), V_T^+(r)$	$V_{LS}^+(r)$

c.m. energies to test this conjecture by a phenomenological analysis.

The data reported here for $\vec{t}$-p elastic scattering fall in the c.m. energy range 1.26 - 3.71 MeV. Hence a phase shift analysis of these data is of great interest for comparison with the calculations of H76. We performed such an analysis using the code CPHASE described by Hardekopf et al.[26] This code calculates cross sections and analyzing powers for the elastic scattering of spin-1/2 projectiles from spin-1/2 targets, starting from complex, J-, s-, and ℓ-dependent phases and real singlet-triplet spin mixing parameters (which simulate the effect of off-diagonal elements of the scattering matrix). The program uses a gradient-search routine to find the phases which best fit the cross section and analyzing power at a single energy, using the usual χ^2 parameter as a fitting criterion.

The only inelastic channel of concern in this energy range is H(t, ^{3}He)n. Total inelastic cross sections for each energy were extracted from the data given by Costello.[28] This cross section was computed from the imaginary components of the phase shifts and fit simultaneously with the cross section and analyzing power angular distributions.

The preliminary best-fit phase shifts are shown in Table VIII. In general, the phases $\delta^J_{L\mathcal{S}}$ and absorption parameters $\eta^J_{L\mathcal{S}}$ behave smoothly, with the exception of a discontinuity in δ^0_{00} and η^1_{10} at 3.21 MeV. The nonzero values for the p-wave mixing parameter at low energies are also somewhat surprising. However, recent measurements of T($\vec{p}$,p)T analyzing powers at Ohio State[27] show significant differences from the LASL H($\vec{t}$,t)H analyzing powers, even at the lowest measured c.m. energy. These differences can be explained, in our formalism, by finite p-wave mixing.

Figures 5 and 6 compare the cross sections and analyzing powers predicted by our best fit phases with the values predicted by H73. At 1.26 MeV, H73 predicts the wrong shape for the cross section, but the agreement can be improved significantly by relatively minor adjustments of the p-wave phases. At 3.71 MeV, only the absolute magnitude of the cross section is missed by H73—a discrepancy which can be corrected by a change in the s-wave phases.

TABLE VIII

BEST-FIT PHASE SHIFTS $\delta^J_{L\mathcal{S}}$, ABSORPTION PARAMETERS $\delta^J_{L\mathcal{S}}$, AND P-WAVE MIXING PARAMETER ϵ FOR H($\vec{t}$,t)H ELASTIC SCATTERING

	1.26 MeV	1.68 MeV	2.19 MeV	2.70 MeV	3.21 MeV	3.71 MeV
δ^0_{00}	−86.6	86.4	81.0	77.4	48.2	77.0
δ^1_{01}	−23.9	−31.7	−33.4	−37.5	−45.5	−43.4
δ^1_{10}	1.0	−2.2	4.0	5.1	7.8	11.2
δ^3_{11}	24.1	33.5	53.1	68.6	75.5	87.8
δ^1_{11}	5.2	14.7	18.0	24.2	35.7	36.9
δ^0_{11}	84.8	135.7	143.8	148.2	157.5	121.9
δ^2_{20}	0.4	6.1	2.9	3.5	4.2	5.7
η^0_{00}	0.32	0.24	0.21	0.24	0.19	0.42
η^1_{01}	1.00	1.00	1.00	0.99	0.99	1.00
η^1_{10}	1.00	0.96	0.78	0.69	0.94	0.55
η^3_{11}	0.84	0.69	0.33	0.27	0.29	0.32
η^1_{11}	1.00	0.97	0.90	0.78	0.65	0.56
η^0_{11}	0.49	0.37	0.27	0.16	0.13	0.13
η^2_{20}	1.00	1.00	1.00	1.00	1.00	0.99
ϵ	−3.5	−7.7	−3.9	−1.6	−3.5	−4.1

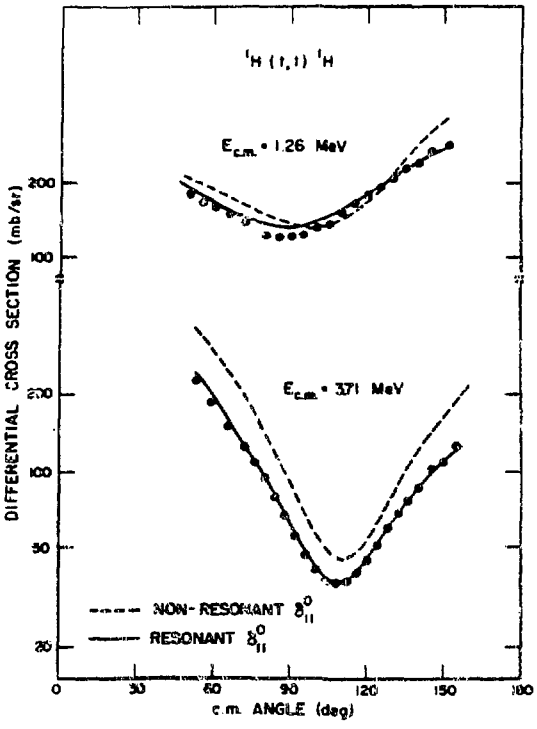

Fig. 5.
Comparison of experimental differential cross sections (solid circles), cluster-model calculations (dashed line), and single-energy phase-shift fits with a resonant δ^0_{11} phase (solid curve).

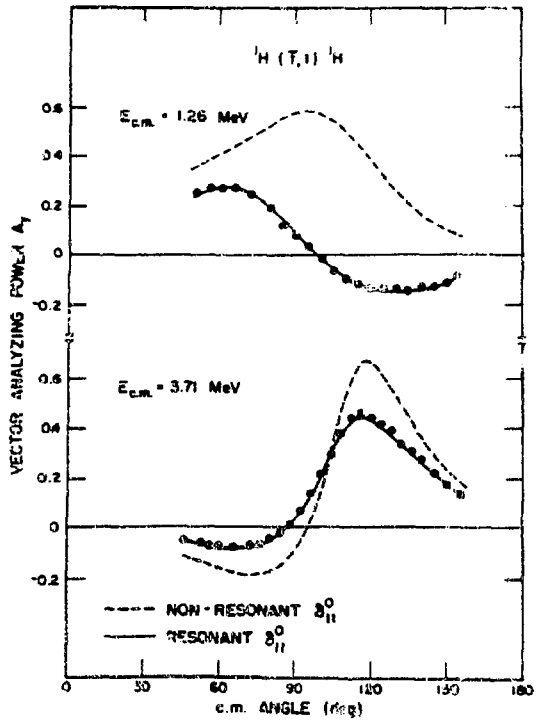

Fig. 6.
Comparison of experimental vector analyzing powers (solid circles), cluster-model calculations (dashed lines), and single-energy phase-shift fits with a resonant δ^0_{11} phase (solid curve).

Hence, the cross sections do not discriminate clearly in favor of either calculation.

However, the analyzing power angular distributions clearly favor the current phase shifts, with their choice of a resonant δ^0_{11} phase. At 3.71 MeV, H73 reproduces the general shape of the A_y angular distribution, but misses the magnitude by a significant amount. At 1.26 MeV, not even the shape of the A_y distribution is correctly predicted by H73, while the phase-shift fit with the resonant 0^- phase follows the data quite well.

Figure 7 shows the δ^0_{11} phase from H76, the best fit δ^0_{11} phase from our phase-shift analysis, and the δ^0_{11} phase derived from an energy-dependent R-matrix analysis of the four-nucleon system.[28] The agreement is sufficient to indicate the necessity of including the odd spin-orbit and tensor forces in the cluster-model calculations.

VI. CONCLUSIONS

The measurement of H($\vec{t}$,t)H elastic scattering reported above was designed to acquire cross section and analyzing power data at energies in the vicinity of the 0^- and 2^- resonances in ^{4}He. These data have been parameterized in terms of complex, J-, ℓ-, and s-dependent phases and a real spin-mixing parameter.

While knowledge of these phenomenological parameters is useful enough by itself, the phase-shift analysis has also allowed us to address a fundamental question about the microscopic calculations on the ^{4}He system carried out by Heiss and Hackenbroich.[21] It is usually assumed (see, for example, Ref. 29) that the "small" components of the nucleon-nucleon interaction—that is, the odd-parity central and tensor forces, and the even-parity

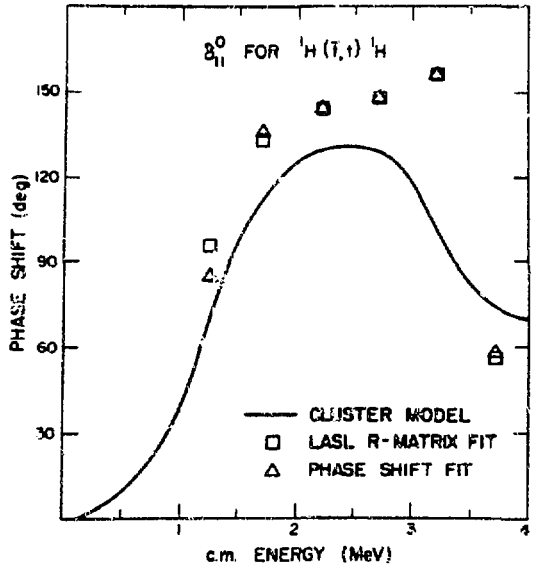

Fig. 7.
Values for the phase δ_{11}^{0} as a function of energy, calculated from a cluster model (solid curve), single-energy phase-shift analysis (open triangles), and an energy-dependent R-matrix calculation (open squares).

spin-orbit force, and tensor forces—can be neglected in such calculations. However, the level-ordering for ^{4}He predicted by the calculations without the "small" forces is wrong. Moreover, as Hackenbroich has shown,[8] the inclusion of these forces has a drastic effect on the 0^- phase for H + t scattering at low energies. This change in the 0^- phase, in turn, changes the predicted ^{4}He level scheme from wrong to right for the odd-parity levels.

By confirming, through a phenomenological analysis, that the 0^- phase must indeed be resonant, we have verified the need for including the "small" internucleon forces in microscopic calculations for ^{4}He.

REFERENCES

1. L. L. Foldy and J. D. Walecka, "Muon Capture in Nuclei," Nuovo Cimento **34**, 1026 (1964).

2. E. Wigner, "On the Consequences of the Symmetry of the Nuclear Hamiltonian on the Spectroscopy of Nuclei," Phys. Rev. **51**, 106 (1937).

3. A. de-Shalit and J. D. Walecka, "Nuclear Spectroscopy in the α Particle," Phys. Rev. **147**, 763 (1966).

4. S. Fiarman and W. E. Meyerhof, "Energy Levels of Light Nuclei A = 4," Nucl. Phys. **A206**, 1 (1973).

5. B. R. Barrett, "Particle-Hole States in the Alpha Particle with Realistic Forces," Phys. Rev. **154**, 955 (1967).

6. R. Kankowsky, J. C. Fritz, K. Kilian, A. Neufert, and D. Fick, "Elastic Scattering of Polarized Protons on Tritons Between 4 and 12 MeV," Nucl. Phys. **A263**, 29 (1976).

7. L. R. Veeser, D. D. Armstrong, and P. W. Keaton, Jr., "Polarization of Tritons Scattered from Hydrogen," Nucl. Phys. **A140**, 177 (1970).

8. H. H. Hackenbroich, "Structure and Reactions of Light Nuclei," in *Proc. 4th Int. Symp. on Polarization Phenomena in Nuclear Reactions*, W. Grüebler and V. König, Eds. (Birkhäuser, Zurich, 1976), p. 133.

9. H. H. Hackenbroich and P. Heiss, "A Microscopic Calculation for n-^{4}H Scattering," Z. Physik **242**, 359 (1971).

10. E. A. Hardekopf, G. G. Ohlsen, R. V. Poore, and Nelson Jarmie, "Location of a Polarization Extremum in Triton-Alpha Scattering and its Application to a New Polarized-Triton Source," Phys. Rev. **C13**, 2127 (1976).

11. P. A. Lovoi, "Proton-Proton Analyzing Power Measurements at 16 MeV," Los Alamos Scientific Laboratory report LA-6041-T (1975).

12. D. D. Armstrong, J. G. Beery, E. R. Flynn, W. S. Hall, P. W. Keaton, Jr., and M. P. Kellogg, "Particle Identification Utilizing an On-Line Computer," Nucl. Inst. Meth. **70**, 69 (1969).

13. G. G. Ohlsen and P. W. Keaton, Jr., "Techniques for Measurement of Spin-1/2 and Spin-1 Polarization Analyzing Tensors," Nucl. Inst. Meth. **109**, 41 (1973).

14. E. A. Silverstein, "Calculation of the G Factor for Gas Scattering Experiments," Nucl. Inst. Meth. **4**, 53 (1959).

15. Nelson Jarmie, J. H. Jett, J. L. Detch, Jr., and R. L. Hutson, "Proton-Proton Elastic Scattering from 9.8 to 13.6 MeV," Phys. Rev. **C3**, 10 (1971).

16. M. Ivanovich, P. G. Young, and G. G. Ohlsen, "Elastic Scattering of Several Hydrogen and Helium Isotopes from Tritium," Nucl. Phys. **A110**, 441 (1968).

17. M. E. Ennis and A. Hemmendinger, "Small-Angle Cross Sections for the Scattering of Protons by Tritons," Phys. Rev. **95**, 772 (1954).

18. G. G. Ohlsen, J. L. McKibben, G. P. Lawrence, P. W. Keaton, Jr., and D. D. Armstrong, "Precise Proton-Polarization Standards Determined with a Lamb-Shift Ion Source Incorporating a Nuclear Spin Filter," Phys. Rev. Lett. **27**, 599 (1971).

19. G. G. Ohlsen, P. A. Lovoi, G. C. Salzman, U. Meyer-Berkhout, C. K. Mitchell, and W. Grüebler, "Analyzing Power for d-^{4}He Elastic Scattering at 12.0, 14.0, and 17.0 MeV," Phys. Rev. C 8, 1262 (1973).

20. E. Huenges, H. Rösler, and H. Vonach, "High-Resolution Time-of-Flight System for Precise Measurements of Excitation Energies and Q-Values," Phys. Lett. **46B**, 361 (1976).

21. N. Bohr, "On the Decrease of Velocity of Swiftly-Moving Electrified Particles in Passing Through Matter," Phil. Mag. **30**, 581 (1915).

22. J. M. Blatt and L. C. Biedenharn, "The Angular Distribution of Scattering and Reaction Cross Sections," Rev. Mod. Phys. **24**, 258 (1952).

23. H. Eikemeier and H. H. Hackenbroich, "A Phenomenological Local Soft-Core Nucleon-Nucleon Potential," Nucl. Phys. **A169**, 407 (1971).

24. P. Heiss and H. H. Hackenbroich, "A Microscopic Calculation for the Reactions ^{3}H(p,p)^{3}H, ^{3}He(n,n)^{3}He and ^{3}H(p,n)^{3}He," Nucl. Phys. **A202**, 353 (1973).

25. R. A. Hardekopf, P. W. Lisowski, T. C. Rhea, R. L. Walter, and T. B. Clegg, "Four-Nucleon Studies (IV), Analyzing Powers in the Elastic Scattering of Protons from Tritium," Nucl. Phys. **A191**, 481 (1972).

26. D. G. Costello, "Review of ^{3}He(n,p)T Reaction," in *Neutron Standards and Flux Normalization*, A. B. Smith, Ed. (Oak Ridge, U.S.A.E.C., 1971), p. 74.

27. T. R. Donoghue, Ohio State University, personal communication, October 1976.

28. G. M. Hale, Los Alamos Scientific Laboratory, personal communication, October 1976.

29. S. Ramavataram, C. L. Rao, and K. Ramavataram, "A Microscopic Description of the Negative-Parity Resonances in the Mass-4 System by the Coupled-Channels Method (II)," Nucl. Phys. **A255**, 109 (1975).